Hindawi
Advances in Civil Engineering
Volume 2019, Article ID 7810542, 9 pages
https://doi.org/10.1155/2019/7810542

Research Article

Improved SDOF Approach to Incorporate the Effects of Axial Loads on the Dynamic Responses of Steel Columns Subjected to Blast Loads

Junbo Yan, Yan Liu, and Fenglei Huang

State Key Laboratory of Explosion Science and Technology, Beijing Institute of Technology, Beijing 100081, China

Correspondence should be addressed to Yan Liu; liuyan@bit.edu.cn

Received 19 September 2018; Revised 15 October 2018; Accepted 15 January 2019; Published 12 February 2019

Academic Editor: Chiara Bedon

In this paper, a complicated single-degree-of-freedom (SDOF) approach was developed to determine the global response of steel columns under combined axial and blast-induced transverse loads. Nonlinear section and member analyses were incorporated into the suggested SDOF method to account for the complex features of the material behavior, the high strain rate effect, and the column geometry. The SDOF technique was validated through comparisons with available finite element and experimental data, and a good consistency was obtained. Then, the validated SDOF approach was utilized to derive the pressure-impulse curves under various levels of axial loading. The level of the axial load was shown to have a significant influence on the dynamic behavior of a steel column subjected to a blast load.

1. Introduction

Recently, increasingly frequent terrorist activities have made blast protection essential for engineering communities [1]. The failure of load-bearing columns can result in the progressive collapse of structures. Therefore, it is important to improve the reliability of vulnerable columns under blasts to ensure the safety of structures [2, 3].

One of the most widely used approaches to assess the effects of blasts on structures is the equivalent single-degree-of-freedom (SDOF) approach. In addition, the efficient SDOF method has proven to be a powerful tool for deriving iso-damage pressure-impulse (P-I) diagrams, which can predict structural damage. For example, several technical manuals such as the unified facilities criteria (UFC) [4] based on linear resistance curves are used to design protective structures subjected to blast loads, and idealized load-deformation characteristics are given in the form of design charts. Dragos and Wu [5] proposed a simplified SDOF approach based on the new concept of a reduced resistance-deflection function to derive the P-I diagram for steel columns. Fallah and Louca [6] proposed analytical formulas for obtaining a normalized P-I diagram based on a simple SDOF method incorporating the linear resistance. Further, Nassr et al. [7] demonstrated the SDOF method's ability to study the response of steel beams subjected to blast loads, and Nassr et al. [8] later employed the SDOF approach to study the axial load effects on steel columns under blast loads. In addition, Wang et al. [9] studied the SDOF approach to evaluate the concrete structural members under close-in nonuniform blast loads, and a comparison with test results indicated that the SDOF method can give reasonable predictions. Bedon et al. [10] carried out the analytical calculations by means of SDOF formulations derived from structural dynamics theories and proposed a design approach for practical estimation of buckling strength of glass elements in the analyzed loading and boundary conditions. Liu et al. [11] performed the field tests to investigate the blast response of steel-reinforced concrete (RC) beams and validate the nonlinear SDOF approach to predict the maximum displacements of RC beams subjected to blast loading. However, the axial load effect was neglected.

Currently, structural elements are typically simplified as having perfectly elastic-plastic force-deformation relationships [7, 8]. However, this idealized member resistance has inherent

limitations for capturing the gradual effect of plastic behavior on the dynamic properties of the system [9, 12]. Therefore, employing this force-deformation characteristic causes some uncertainty in the calculations.

Further, in reality, when subjected to a lateral blast pressure, an axial load tends to induce additional lateral deformation and magnify bending within a column. Thus, a structural response to blast loads that ignores axial load effects may not very accurately reflect the true behavior of a structure [13].

In this paper, a more accurate and sophisticated flexural behavior (featuring both the moment-curvature relationship and the force-deformation relationship) that considers the complex features of the slab geometry and the material's behavior under high strain rate loading is incorporated into a nonlinear SDOF approach for the dynamic analysis of columns subjected to blast-induced shock waves under various levels of axial compressive loads.

This approach also has the capability to generate iso-contour P-I diagrams of blast-loaded columns. To validate the suggested SDOF approach, the structural load-deformation characteristics, predicted maximum displacements, and iso-displacement P-I diagrams in this paper were compared against experimental and finite element model (FEM) results from [5, 14], respectively.

2. Theoretical Analyses of the Response of a Steel Column

2.1. Sectional Analysis. Assuming that plane sections remain planar under purely flexural behavior, a sectional analysis is performed to compute the moment-curvature characteristics for use in member analysis [15] as shown in Figure 1.

A solution procedure to generate the moment-curvature is outlined below, as shown in Figure 2.

(1) The cross section of the column is divided into a desirable number of slices n parallel to the column axis.

(2) Strain values ε_{top} are specified for the extreme steel compression fiber, and a corresponding depth x_{n} for the neutral axis is selected. The strain profile within the section is then generated:

$$\varepsilon_i = \frac{x_i}{x_{\text{n}}}\varepsilon_{\text{top}}, \tag{1}$$

where x_i is the distance between the corresponding layer and the neutral axis.

(3) After the strain profile within the section is generated, the internal forces on the cross section are generated by employing the material's stress-strain relationships:

$$N_i = bh_i\sigma_i, \tag{2}$$

where b is the width of the section, σ_i is the stress on the i-th layer of the steel, and h_i is height of the i-th layer of the section.

(4) The depth of the neutral axis is revised until the difference between the applied axial load N and the resultant internal force is within a convergence criterion:

$$\sum_i^n \sigma_i \Delta A_i = N, \tag{3}$$

where ΔA_i is the area of the i-th layer of the section.

(5) The resulting moments and curvatures are then calculated using these internal forces and strain profiles:

$$M = \sum_i^n \sigma_i \Delta A_i x_i, \qquad \phi = \frac{\varepsilon_{\text{top}}}{x_{\text{n}}}. \tag{4}$$

(6) Another incremental extreme compression fiber strain is selected, and the procedure is repeated until the extreme compression of concrete up to its ultimate compressive strain is reached for a given axial load.

2.2. Material Modeling. The stress-strain relationships of the member's material are incorporated into a member analysis to relate the member's deformation to the developed internal forces. The stress-strain curve is identical to the material properties described in [15], which have been thoroughly validated.

2.2.1. Steel. Compressive stress-strain relationships are assumed to be the same as tensile stress-strain relationships. The stress-strain relationship for reinforcing steel in tension consists of two linear segments, as shown in Figure 3.

2.2.2. High Strain Rate Effect on Steel. Accounting for the effects of high strain rates is critical in the analysis and design of members subjected to blast loads, as materials experience an increase in strength under high strain rates. The dynamic increase factor, DIF, is defined as the ratio of the dynamic material strength to the static material strength. Based on the relationship proposed by Malvar and Crawford [16], the dynamic material increase factors for both the yield strength and the ultimate strength are given by the following:

$$\text{DIF} = \left(\frac{\dot{\varepsilon}_{\text{s}}}{10^{-4}}\right)^{\alpha}, \tag{5}$$

where the DIF for the yield strength of steel may be determined by substituting $\alpha = \alpha_{f_{\text{y}}}$ into equation (5) as follows:

$$\alpha_{f_{\text{y}}} = 0.074 - \frac{0.040 f_{\text{y}}}{414}, \tag{6}$$

where f_{y} is the static yield strength of steel (in MPa). Similarly, the DIF for the ultimate strength of steel may be determined by substituting $\alpha = \alpha_{f_{\text{u}}}$ in equation (5) as follows:

$$\alpha_{f_{\text{u}}} = 0.019 - \frac{0.009 f_{\text{u}}}{414}. \tag{7}$$

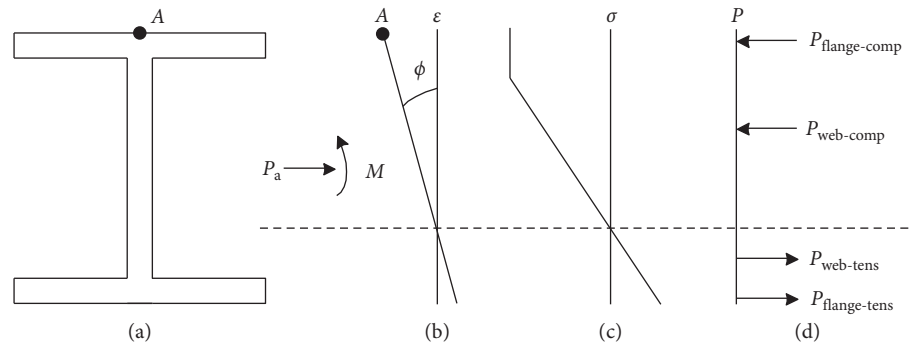

Figure 1: Moment-curvature analysis for a section. (a) Cross section. (b) Strain. (c) Stress. (d) Force.

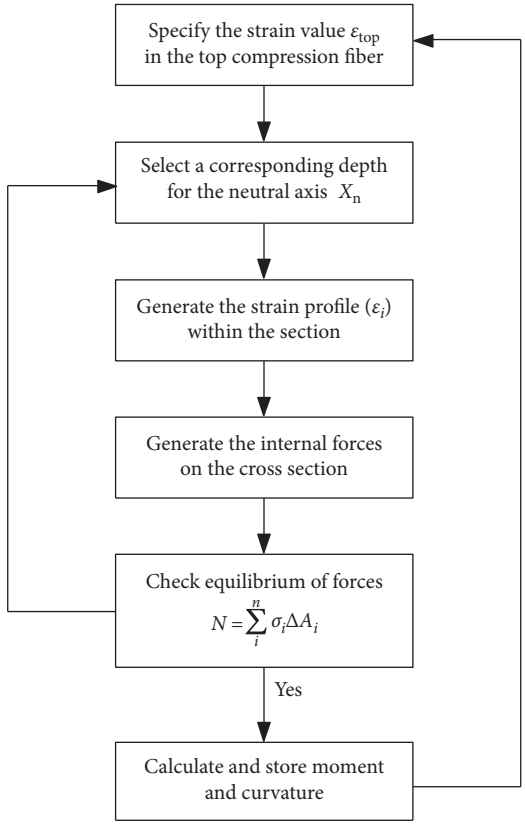

Figure 2: Flow chart of the numerical procedure for section analysis.

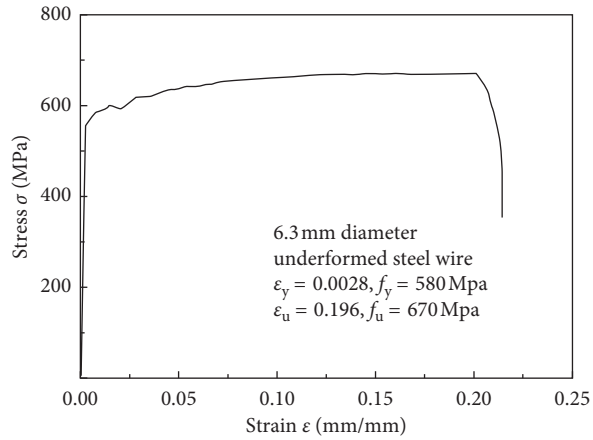

Figure 3: Tensile stress-strain relationship of steel.

2.3. Member Analysis. To capture the full time history response of a steel-reinforced concrete column subjected to dynamic loading, the complete force-displacement relationship rather than the ultimate resistance is needed. The moment-curvature curve generated by sectional analysis is used to perform the member analysis of the steel-reinforced columns.

The following discussion outlines a procedure for obtaining the complete nonlinear resistance functions for steel concrete columns, which is also shown in Figure 4:

(1) Establish the moment-curvature relationship for the section. A column with a length l is divided equally into a desirable number of segments (equal to m), each of which has a length Δl, as shown in Figure 5. Assume a curvature on the midspan of the column φ_m; the initial φ_m is zero, and at every step, $\varphi_m = \varphi_m + \Delta\varphi$. The moment M_m on the midspan is then computed based on the moment-curvature relationships.

$m = 500$ was used for the analysis. Convergence study shows that further decrease of mesh size only has little effect on the numerical results but leads to a much longer calculation time.

(2) Assume an initial incremental distributed deflection $\delta_{i,k}$ $(i = 0, 1, \ldots, m)$.

(3) The assumed horizontal load P is calculated by the axial load P_a, M_m, and $\delta_{i,0}$:

$$P = \frac{2\left(M_m - P_a \delta_{i,k}\right)}{l}. \tag{8}$$

(4) The incremental distributed moment M_i is calculated by P, P_a, and $\delta_{i,k}$. Then, the distributed curvature φ_i is determined based on the moment-curvature relationship:

$$M_i = P \cdot x_i + P_a \cdot \delta_{i,k}. \tag{9}$$

(5) In the conjugate column method, each segment divided above is considered a small imaginary column having the same length as the original segment. The midspan displacement of the segment can be calculated by the following expression:

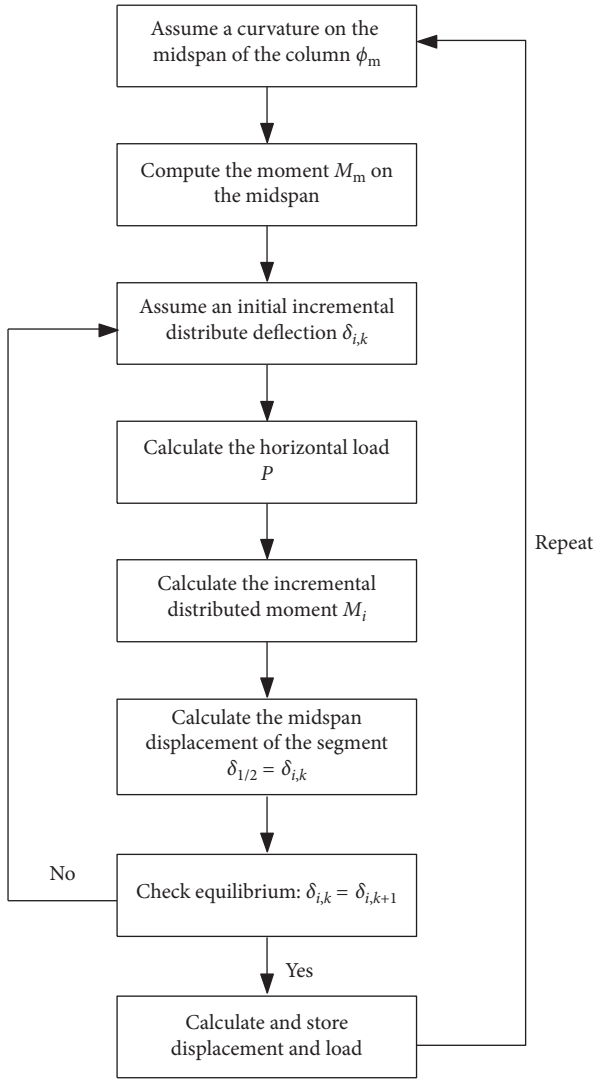

Figure 4: Flow chart of the numerical procedure for calculating the resistance function.

$$\delta_{l/2} = \delta_{i,k} = \sum_{i=1}^{m/2} \varphi_i \Delta x \left(\frac{l}{2} - x_i \right). \tag{10}$$

(6) Assume the new incremental distributed deflection is $\delta_{i,k+1}$, repeat steps (4)-(6), and then determine $\delta_{i,2}$, $\delta_{i,3}$, $\ldots \delta_{i,k}$, $\delta_{i,k+1}$. If $\delta_{i,(k+1)}$ and $\delta_{i,k}$ are close enough (where the difference is less than an allowable value), then enter the next cycle. Finally, the whole load-deflection curve is determined [1].

2.4. Dynamic SDOF Analysis. The dynamic response of the columns was predicted using dynamic inelastic single-degree-of-freedom (SDOF) analysis after defining the nonlinear resistance curve for the structure [11] The SDOF system is shown in Figure 6.

The idealized SDOF system is described by the following equation of motion:

$$K_M M \ddot{x}(t) + K_L R(x(t)) = K_L F_c(t), \tag{11}$$

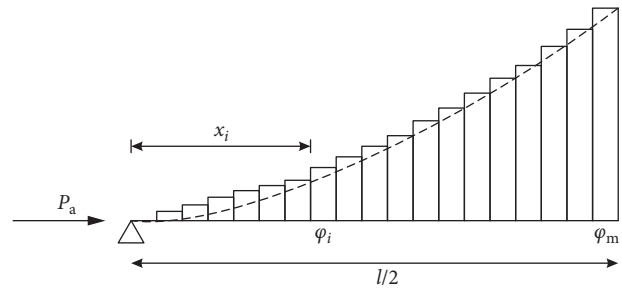

Figure 5: Member analysis.

where $x(t)$ and $\ddot{x}(t)$ represent the displacement and acceleration, respectively, of the column at the midspan, M is the mass of the column, $R(x)$ is the resistance as a function of the displacement, and $F_c(t)$ is the loading as a function of time.

K_M is the mass factor required to transfer a system with a distributed mass into an equivalent SDOF system and is computed by the following equation:

$$K_M = \frac{\int_0^L \overline{m} \varphi(x)^2 \, dx}{\overline{x} L}, \tag{12}$$

where $\overline{m}$ is the mass per unit length of the member and $\Phi(x)$ is the shape function of the member.

K_L is the load factor used to transform the distributed force and stiffness into a single point load and is defined as follows:

$$K_L = \frac{\int_0^L F \varphi(x) \, dx}{\mathrm{FL}}. \tag{13}$$

It is convenient to define a load mass factor [2], K_{LM}, as a ratio of the mass factor to the load factor:

$$K_{LM} = \frac{K_M}{K_L}. \tag{14}$$

Moreover, the response of the system may be written as follows by incorporating the axial load effect:

$$K_{LM} M \ddot{x}(t) + R(x) = F_c(t) + \frac{8 P_a}{L} x, \tag{15}$$

where P_a is the axial load. The load mass transformation factor, K_{LM}, is defined based on the Biggs analysis [17].

Newmark proposed the following numerical solution technique for this equation [18]:

(1) Assume that y, $\dot{y}$, and $\ddot{y}$ are known at the time $t = t_i$ and assign them the subscript i.

(2) $t_{i+1} = t_i + \Delta t$ and assume a value $\ddot{y}_{i+1}$ for the acceleration at time t_{i+1}, $\dot{y}_{i+1} = \dot{y}_i + (\ddot{y} + \ddot{y}_{i+1})(\Delta t/2)$.

(3) Compute a velocity at t_{i+1}, $\dot{y}_{i+1} = \dot{y}_i + (\ddot{y} + \ddot{y}_{i+1})(\Delta t/2)$. Compute a displacement at t_{i+1}, $y_{i+1} = y_i + \dot{y}_i \Delta t + ((1/2) - \beta) \ddot{y}_i (\Delta t)^2 + \beta \ddot{y}_{i+1} (\Delta t)^2$.

(4) Substitute y_{i+1} and $\dot{y}_{i+1}$ into the above equation and compute a new value for $\ddot{y}_{i+1}$.

(5) Check whether $\ddot{y}_{i+1}$ from step 2 is sufficiently close to $\ddot{y}_{i+1}$ from step 5. If they are sufficiently close, the

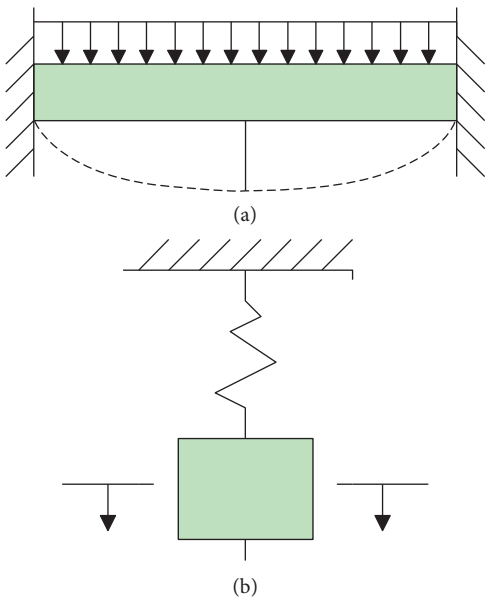

Figure 6: SDOF system. (a) Real structure. (b) Equivalent SDOF system.

solution is achieved. If they are not close, repeat steps 2 through 6 until convergence is attained. Since one needs to assume a new value for $\ddot{y}_{i+1}$ in step 2, it is quite efficient to select the value obtained in step 5 for this purpose.

The β factor determines how the acceleration changes within a time step. In step 2, it is assumed that $\ddot{y}$ varies linearly over Δt. Thus, the default value for β is 1/6 [19].

2.5. P-I Diagram. A P-I diagram as an iso-response curve is typically employed to assess the dynamic response of a structure subjected to a blast load. P-I curves consist of combinations of the peak reflected overpressure and the impulse that cause the same damage level based on a predefined failure mode.

For this study, the midspan displacement of the column is considered the damage criterion. One point on the P-I diagram is generated by specifying an initial positive load duration and iterating a reflected overpressure until the maximum midspan displacement predicted by the SDOF analysis reaches the predetermined damage value.

3. Analysis of Blast-Loaded Steel Columns

3.1. Validation of the SDOF Method Using FEM Results Available in [1]. Dragos and Wu [5] performed an FE analysis of two steel columns under blast loads. One of the two steel columns presented in [5] was also utilized in this study to validate the present SDOF approach. The span of the abovementioned steel column was 4 m, and the width and thickness of the flanges were 102 mm and 10.3 mm, respectively. The columns were simply supported. The total depth of the section was 160 mm, and the thickness of the web was 6.6 mm. The yield strength and Young modulus of the steel specimens were 470 MPa and 180 GPa, respectively.

A 359 kPa reflected pressure and 23.88 ms positive blast duration for the blast conditions were chosen for the calculation. The maximum displacements of the steel column specimens under an axial load of 350 kN were calculated by employing the proposed SDOF analysis.

Figure 7 shows a comparison of the deflection time history between the calculated and FEM results [5]. The calculated and FEM midspan maximum displacements of the steel column are 208.3 mm and 207.7 mm, respectively. However, a significant discrepancy occurs in the initial portions of the midspan deflection histories by both analyses. The negligence of membrane action and damping effects is a possible reason for the significant discrepancies in the initial portions of the midspan deflection histories by both analyses.

P-I diagrams for the maximum midspan displacement of 208.8 mm calculated above using the proposed SDOF approach were generated under an axial load of 350 kN. Figure 8 compares the P-I diagram of a column obtained by the proposed method with the FEM results available in [5]. As the figure illustrates, the P-I combination in the present SDOF analysis is very close to the FEM results from [5]. This result indicates that the present SDOF model gives a reliable prediction of the P-I diagram of a steel column subjected to blast loads.

3.2. Validation of the SDOF Method Using the Experimental Results in [14]. To further validate the accuracy of the abovementioned SDOF approach, maximum midspan displacements generated from the proposed SDOF analysis were compared with the results of the test reported by Nassr et al. [14].

Thirteen typical wide-flange steel columns with two different section sizes, W150 × 24 and W200 × 71, were chosen by Nassr et al. [14] to investigate the dynamic responses of the steel columns to blast loads. Only the steel columns with a section size of W150 × 24 and a height of 2413 mm under the blast conditions in shot 1 and shot 3 are analyzed herein. All of the steel columns were pinned at the top and supported by rollers at the bottom. Therefore, the load mass factor, K_{LM}, was taken as being equal to 0.78 and 0.66 before and after yielding, respectively. The axial load in the experiment was 270 kN for the two specimens.

Figure 9 shows the layouts of the steel column's sections [14]. The static nominal yield strength and ultimate strength of the test specimens were 393 and 537 MPa, respectively. In shot 1, a charge size of 50 kg at a stand-off distance of 10.3 m was used to generate the blast environment. The average of the measured reflected pressures was 307 kPa, and the positive phase duration had an average value of 7.3 ms. In shot 3, a pressure time history was obtained by a charge size of 150 kg at a stand-off distance of 9 m. The peak pressure and positive phase

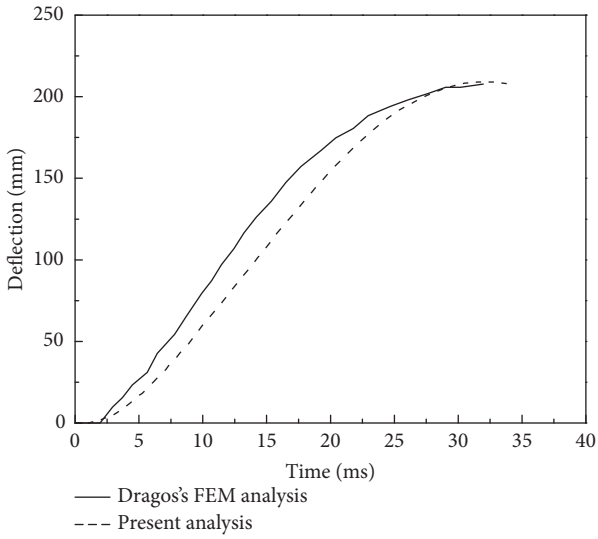

Figure 7: Comparison of the midspan displacements for blast no. 1.

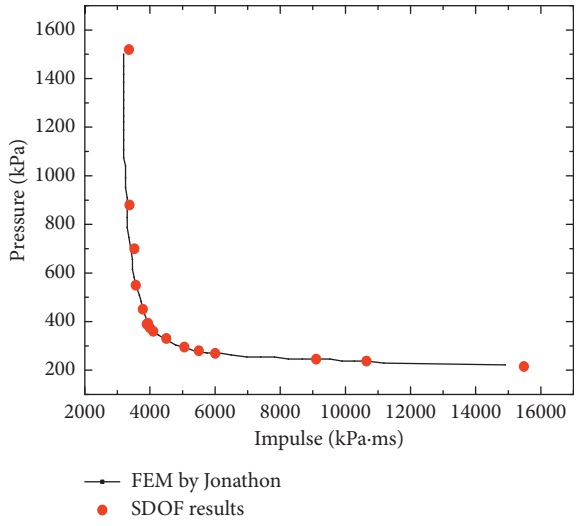

Figure 8: Comparison of P-I diagrams.

duration were 1560 kPa and 6.2 ms, respectively. A typical reflected pressure time history obtained in shot 1 is shown in Figure 10.

Comparisons of the calculated and test deflection time histories at the middle of the column are shown in Figure 11. The differences in the maximum deflections between the present analysis and experiments are 2.5% and 2.6% for shot 1 and shot 3, respectively. This result indicates that the SDOF model also gives reliable predictions of the responses of steel columns to blast loads. However, significant discrepancies occur in the initial portions of the midspan deflection histories by both analyses. The difference in the load-time histories under the real blast load and the SDOF analysis represents one possible reason for the reduced accuracy. The reflected pressure as a function of time was modeled using an equivalent triangular blast load having the same peak reflected pressure and impulse found

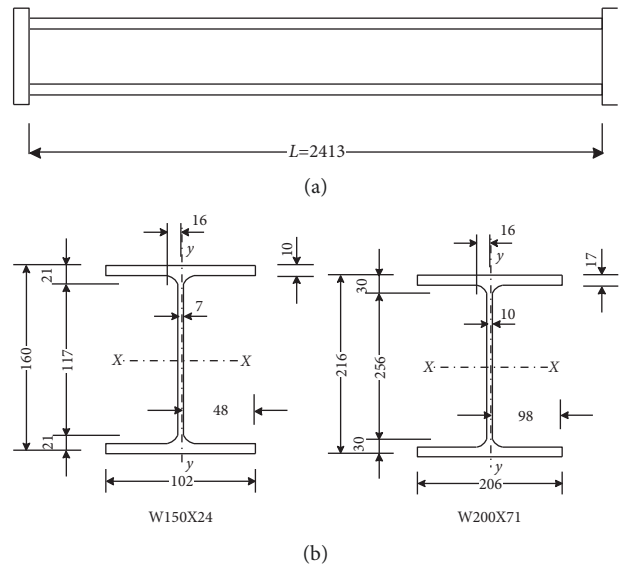

Figure 9: (a) Test specimens and (b) cross sections of the test specimens.

in the experiments. Thus, more accurate load-time histories should be employed. In addition, the shear damage mode is not considered in the present study; accordingly, a more accurate SDOF model considering other damage modes should be analyzed in further research.

3.3. Effects of Axial Loads. When a column is subjected to blast loads, the static compressive axial load induced by the gravity load affects the dynamic response of the column. The specimen analyzed above (W150 × 24) and the blast conditions (shot 1 and shot 3) available in [14] were employed here to investigate the effects of axial loads on the dynamic responses of steel columns. The effects of axial loads were investigated by applying three different axial loads, namely, 0 kN, 270 kN, and 400 kN.

3.3.1. Effects of Axial Loads on the Maximum Displacements. Figure 12 illustrates the effects of different axial loads on the displacement responses of columns under various load conditions. When the impulsive loading and corresponding deformation are small, the midspan displacement decreases with an increase in the axial load because the axial load amplifies the moment capacity of the column. However, when the column experiences large deformation, an increasing axial load results in a greater midspan displacement. This is caused by the P-Δ effect, which is that when a column is subjected to both lateral and axial loading, the axial load creates an additional bending moment and thus enhances the lateral deflection of the column. The blast load induces lateral deformation in the column, causing the applied and resisting axial forces to form a couple, as they are no longer collinear. This couple causes additional lateral deformation and bending in the column, thereby inducing a greater midspan displacement.

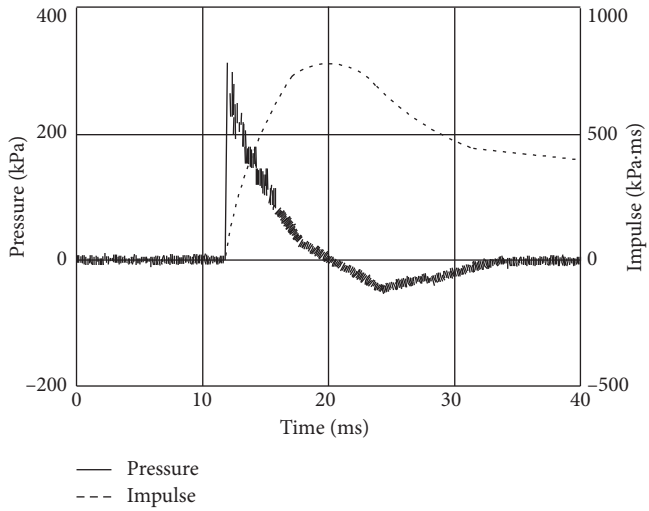

Figure 10: A typical reflected pressure time history obtained in shot 1.

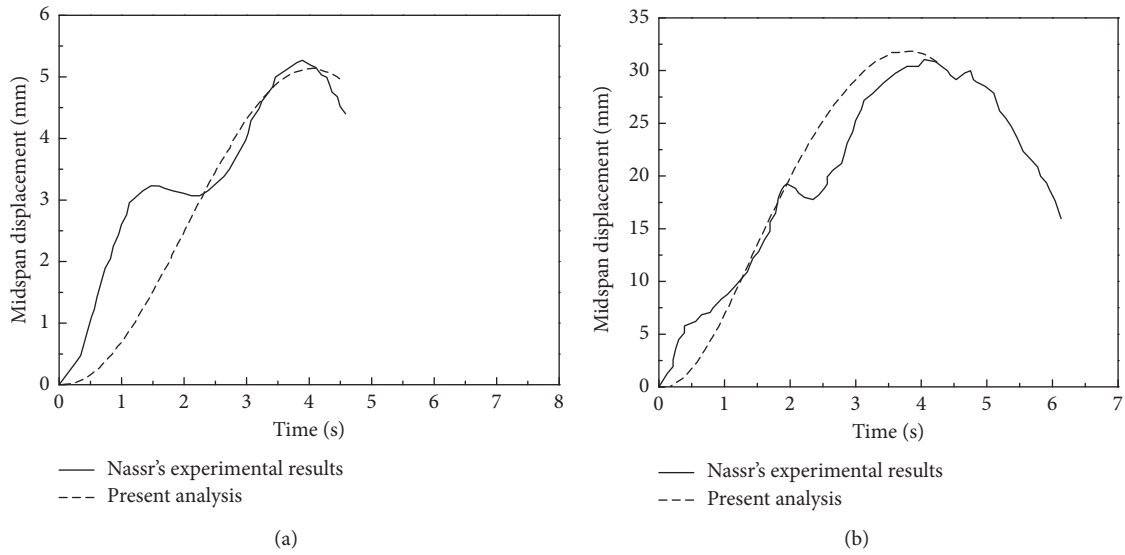

Figure 11: Experimental midspan displacements plotted against those predicted by SDOF analysis. (a) Comparison of the midspan displacements for shot 1. (b) Comparison of the midspan displacements for shot 3.

3.3.2. Effects of Axial Loads on P-I Diagrams. To investigate the effects of axial loads on the P-I diagram of a steel column, P-I diagrams were generated under the abovementioned axial loads. The maximum midspan displacements of 10 mm and 90 mm were determined as damage criteria.

Both P-I diagrams are shown in Figure 13. As seen from Figure 13(a), with a decrease in the axial load applied to the columns, the P-I diagram shifts to the left. This result indicates that an increase in the axial load can increase the ability of a column to resist blast loads. However, Figure 13(b) indicates that a larger axial load can decrease the ability of a steel column to resist blast loads when the maximum midspan displacement is large because of the P-Δ effect.

4. Conclusion

In this paper, an SDOF model was developed to determine the global response of blast-loaded steel columns. The model also incorporates nonlinear moment-curvature and force-deformation relationships instead of a perfectly linear elastic-plastic force-deformation relationship. The proposed member analysis accounted for the material constitutive model, the strain rate effects, the gradual effect of the formation and progression of plastic behavior, and the effects of various axial loads. To validate the SDOF method, the theoretical SDOF maximum displacements were compared with the FEM and experimental results in [5, 14], respectively. The results

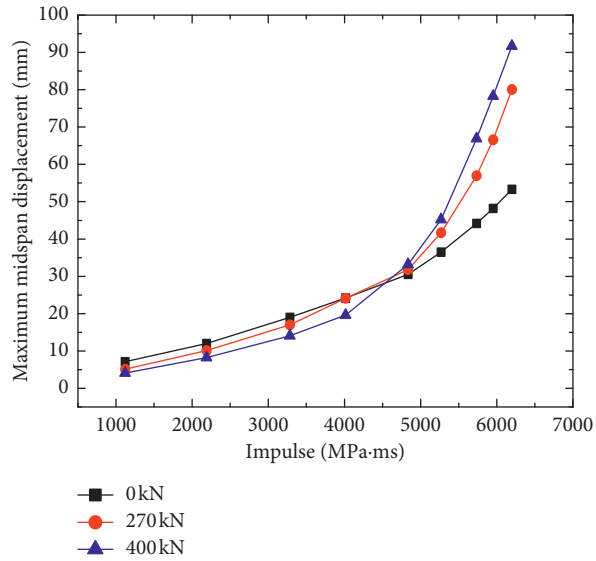

Figure 12: Effects of axial loads on the displacement responses of columns under various load conditions.

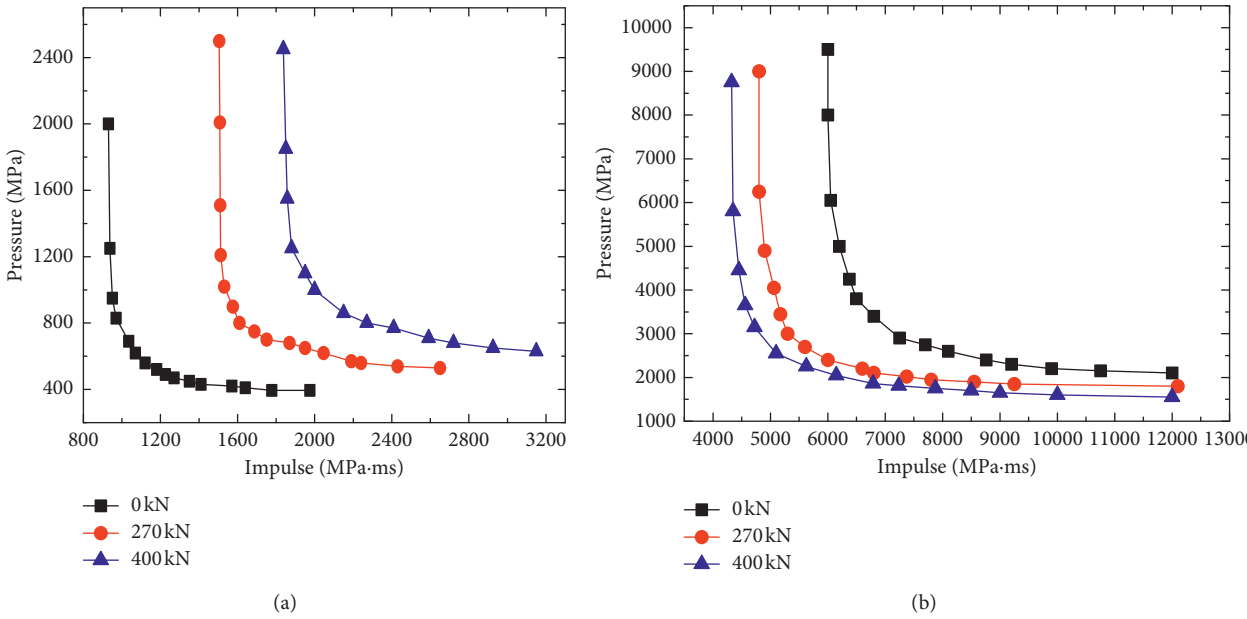

Figure 13: P-I curves for varying axial loads. (a) P-I curves for a 10 mm midspan displacement. (b) P-I curves for a 90 mm midspan displacement.

agreed well, indicating that the proposed SDOF model can accurately predict the deflection and P-I diagram of a blast-loaded column.

The maximum midspan displacements and P-I diagrams for steel columns under various axial loads were generated based on the proposed SDOF approach. The level of the axial compressive load was found to have a significant effect on the response of a steel column. When the level of the blast load is small, an increase in the axial load can reduce the maximum displacement and enhance the ability of the column to resist the blast load, which is caused by the enhanced moment capacity induced by the axial load. However, when the level of the blast load is sufficiently large, an increase in the axial load can increase the maximum displacement and reduce the ability to resist the blast load, which is caused by the P-D effect.

Data Availability

The origin data used to support the findings of this study are included within the article. The Matlab code data used to support the findings of this study were supplied by Junbo Yan under license and thus cannot be made freely available. Requests for access to these data should be made to Junbo Yan (e-mail address: 3120140060@bit.edu.cn).

Conflicts of Interest

The authors declare that there are no conflicts of interest regarding the publication of this paper.

Acknowledgments

This paper was supported by the National Natural Science Foundation of China under grant nos. 11390362 and 11221202.

References

[1] J. Dragos, C. Wu, M. Haskett, and D. Oehlers, "Derivation of normalized pressure impulse curves for flexural ultra high performance concrete slabs," *Journal of Structural Engineering*, vol. 139, no. 6, pp. 875–885, 2012.

[2] S. Astarlioglu, T. Krauthammer, D. Morency, and T. P. Tran, "Behavior of reinforced concrete columns under combined effects of axial and blast-induced transverse loads," *Engineering Structures*, vol. 55, pp. 26–34, 2013.

[3] A. Echevarria, A. E. Zaghi, V. Chiarito, R. Christenson, and S. Woodson, "Experimental comparison of the performance and residual capacity of CFFT and RC bridge columns subjected to blasts," *Journal of Bridge Engineering*, vol. 21, no. 1, article 04015026, 2015.

[4] United States Department of Defense, "Unified facilities criteria: design of buildings to resist progressive collapse," in *UFC 4-023-03*, United States Department of Defense, Washington, DC, USA, 2009.

[5] J. Dragos and C. Wu, "Single-degree-of-freedom approach to incorporate axial load effects on pressure impulse curves for steel columns," *Journal of Engineering Mechanics*, vol. 141, no. 1, article 04014098, 2014.

[6] A. S. Fallah and L. A. Louca, "Pressure-impulse diagrams for elastic-plastic-hardening and softening single-degree-of-freedom models subjected to blast loading," *International Journal of Impact Engineering*, vol. 34, no. 4, pp. 823–842, 2007.

[7] A. A. Nassr, A. G. Razaqpur, M. J. Tait, M. Campidelli, and S. Foo, "Strength and stability of steel beam columns under blast load," *International Journal of Impact Engineering*, vol. 55, pp. 34–48, 2013.

[8] A. A. Nassr, A. G. Razaqpur, M. J. Tait, M. Campidelli, and S. Foo, "Dynamic response of steel columns subjected to blast loading," *Journal of structural engineering*, vol. 140, no. 7, article 04014036, 2013.

[9] W. Wang, D. Zhang, F. Lu, S.-C. Wang, and F. Tang, "Experimental study on scaling the explosion resistance of a one-way square reinforced concrete slab under a close-in blast loading," *International Journal of Impact Engineering*, vol. 49, pp. 158–164, 2012.

[10] C. Bedon, C. Amadio, and A. Sinico, "Numerical and analytical investigation on the dynamic buckling behavior of glass columns under blast," *Engineering Structures*, vol. 79, pp. 322–340, 2014.

[11] Y. Liu, J.-b. Yan, and F.-l. Huang, "Behavior of reinforced concrete beams and columns subjected to blast loading," *Defence Technology*, vol. 14, no. 5, pp. 550–559, 2018.

[12] E. Jacques, A. Lloyd, and M. Saatcioglu, "Predicting reinforced concrete response to blast loads," *Canadian Journal of Civil Engineering*, vol. 40, no. 5, pp. 427–444, 2012.

[13] M. Colombo and P. Martinelli, "SDOF models for RC and FRC circular plates under blast loads," *Applied Mechanics and Materials*, vol. 82, pp. 440–445, 2011.

[14] A. A. Nassr, A. G. Razaqpur, M. J. Tait, M. Campidelli, and S. Foo, "Experimental performance of steel beams under blast loading," *Journal of Performance of Constructed Facilities*, vol. 26, no. 5, pp. 600–619, 2011.

[15] E. Jacques, *Blast Retrofit of Reinforced Concrete Walls and Slabs*, University of Ottawa, Ottawa, Canada, 2011.

[16] L. J. Malvar and J. E. Crawford, "Dynamic increase factors for concrete," in *Naval Facilities Engineering Service Center Port Hueneme CA*, 1998.

[17] J. M. Biggs and B. Testa, *Introduction to Structural Dynamics*, McGraw-Hill, New York, NY, USA, 1964.

[18] N. M. Newmark, "A method of computation for structural dynamics," *Journal of the engineering mechanics division*, vol. 85, pp. 67–94, 1959.

[19] T. Krauthammer, *Modern Protective Structures*, CRC Press, Boca Raton, FL, USA, 2008.